

# Continuous Adjoint in Shape & Topology Optimization – Recent Developments & Applications

K. C. Giannakoglou, E. M. Papoutsis-Kiachagias, I. S. Kavvadias, K. Th. Gkaragkounis  
National Technical University of Athens, Greece  
School of Mechanical Engineering, Parallel CFD & Optimization Unit  
e-mail : kgianna@central.ntua.gr

## Summary:

Research activities at the Parallel CFD & Optimization Unit of NTUA (PCOpt/NTUA) include the development of adjoint-based methods for solving aero- and hydrodynamic shape and topology optimization problems. Recent achievements in the development of continuous adjoint methods are overviewed, prior to illustrating some industrial applications. Without loss in generality, all developments are demonstrated for the incompressible flow model and all computations performed within OpenFOAM®.

Up to recently, regarding the mathematical formulation of continuous adjoint methods, two different approaches were available. The first one expresses the gradient in terms of only boundary/surface integrals, is computationally cheap but, depending on the case, may compute inexact gradients on inadequately stretched grids. The second one expresses the gradient in terms of both surface and field integrals, is very accurate, though computationally much more expensive. To bridge the gap between them, a new enhanced formulation [5] assisted by the adjoint to a grid displacement model is showcased. The new formulation is both accurate and cheap as it is free of volume integrals

In addition, the development of the continuous adjoint method for problems governed by the Reynolds-Averaged Navier-Stokes (RANS) equations, assisted by a PDE-based turbulence model, is presented. The majority of continuous adjoint methods make the assumption of "frozen turbulence", i.e. they refrain from differentiating the turbulence model PDEs and this might become a source of inaccuracies, sometimes even leading to wrongly signed sensitivity derivatives. The differentiation of the most frequently used turbulence models (Spalart–Allmaras [13] also with the use of wall functions [14],  $k-\epsilon$  [12] and  $k-\omega$  SST [4]) as part of the adjoint method formulation, along with the resulting benefits are briefly discussed and demonstrated.

Over and above to the few examples presented to convince the reader about the need to use the above formulations, some cases related to the use of shape and topology optimization for automotive applications follow [10].

## 1 Continuous Adjoint Formulations for Shape Optimization

The derivation of the adjoint equations, their corresponding boundary conditions and the sensitivity derivative (SD) expression, concerning a laminar flow governed by the steady incompress-

ible Navier-Stokes, starts by defining the augmented objective function

$$L = J + \int_{\Omega} u_i R_i^v d\Omega + \int_{\Omega} q R^p d\Omega \quad (1)$$

where  $b_n$ ,  $n = 1, \dots, N$  are the design variables and  $J$  is the objective function. Assuming that  $J$  is defined only along the boundary  $S$  of the flow domain  $\Omega$ , a general way to present it is in the form  $J = \int_S J_{S,i} n_i dS = \int_{S_W} J_{S_W,i} n_i dS + \int_{S_O} J_{S_O,i} n_i dS$  where  $S = S_W \cup S_O$ ,  $S_W$  is the controlled solid wall,  $S_O$  any other boundary of  $\Omega$  and  $n_i$  the outward unit normal vector to  $S$ . Apart from  $J$ ,  $L$  includes also the integrals of the residuals of the momentum ( $R_i^v = 0$ ) and continuity ( $R^p = 0$ ) equations multiplied by the fields of the adjoint velocities  $u_i$  and the adjoint pressure  $q$ . A literature survey shows that the continuous adjoint method can be formulated in two different ways, which both give the same adjoint field equations and boundary conditions, yet different expressions for the gradient of  $J$  with respect to (w.r.t.)  $b_n$ . Recently, a new formulation, [5], which combines the advantages of both, has been developed by PCopt/NTUA.

The first published formulation, leads to gradient expressions with field integrals (FI) including the variations in the spatial coordinates  $\vec{x}$  w.r.t.  $\vec{b}$ , a.k.a. grid sensitivities. The standard way to compute  $\delta\vec{x}/\delta\vec{b}$  is through finite differences (FD) at a cost that scales linearly with the number of design variables. To set-up the *FI* formulation, one should start by the total derivative of  $L$ , i.e.

$$\frac{\delta L}{\delta b_n} = \frac{\delta J}{\delta b_n} + \int_{\Omega} \left( u_i \frac{\delta R_i^v}{\delta b_n} + q \frac{\delta R^p}{\delta b_n} \right) d\Omega + \int_{\Omega} (u_i R_i^v + q R^p) \frac{\delta(d\Omega)}{\delta b_n} \quad (2)$$

where, the last term vanishes since  $R_i^v = R^p = 0$  in  $\Omega$ . By developing the total derivatives of  $R_i^v$  and  $R^p$  w.r.t.  $b_n$ , the corresponding derivatives of  $p$ ,  $v_i$ ,  $\tau_{ij}$  w.r.t.  $b_n$  (where  $\tau_{ij}$  are the components of the stress tensor) and their spatial derivatives appear. By applying the chain rule, the formula  $\frac{\delta}{\delta b_n} \left( \frac{\partial \Phi}{\partial x_j} \right) = \frac{\partial}{\partial x_j} \left( \frac{\delta \Phi}{\delta b_n} \right) - \frac{\partial \Phi}{\partial x_k} \frac{\partial}{\partial x_j} \left( \frac{\delta x_k}{\delta b_n} \right)$  and the Green-Gauss theorem, integrals of expressions multiplied by  $\delta v_i / \delta b_n$  and  $\delta p / \delta b_n$  arise. By zeroing those expressions in the volume integrals of  $\delta L / \delta b_n$  the field adjoint equations are derived, [10]. The adjoint boundary conditions are derived by zeroing the expressions multiplying by  $\delta p / \delta b_n$ ,  $\delta v_i / \delta b_n$  and  $\delta \tau_{ij} / \delta b_n$  in the surface integrals of  $\delta L / \delta b_n$ . The remaining terms in  $\delta L / \delta b_n$  yield the SD expression which reads

$$\frac{\delta J}{\delta b_n} \Big|_{FI} = \int_{\Omega} \left\{ -u_i v_j \frac{\partial v_i}{\partial x_k} - u_j \frac{\partial p}{\partial x_k} - \tau_{ij}^a \frac{\partial v_i}{\partial x_k} + u_i \frac{\partial \tau_{ij}}{\partial x_k} + q \frac{\partial v_i}{\partial x_k} \right\} \frac{\partial}{\partial x_j} \left( \frac{\delta x_k}{\delta b_n} \right) d\Omega + W(0) \quad (3)$$

where

$$\begin{aligned} W(\phi) = & \int_{S_W} J_{S_W,i} \frac{\delta(n_i dS)}{\delta b_n} - \int_{S_W} \left( -u_k n_k + \frac{\partial J_{S_W,k}}{\partial \tau_{lz}} n_k n_l n_z \right) \left( \tau_{ij} \frac{\delta(n_i n_j)}{\delta b_n} + \phi \frac{\partial \tau_{ij}}{\partial x_k} \frac{\delta x_k}{\delta b_n} n_i n_j \right) dS \\ & - \int_{S_W} \frac{\partial J_{S_W,k}}{\partial \tau_{lz}} n_k t_l^I t_z^I \left( \tau_{ij} \frac{\delta(t_i^I t_j^I)}{\delta b_n} + \phi \frac{\partial \tau_{ij}}{\partial x_k} \frac{\delta x_k}{\delta b_n} t_i^I t_j^I \right) dS \\ & - \int_{S_W} \left( \frac{\partial J_{S_W,k}}{\partial \tau_{lz}} n_k (t_l^{II} t_z^I + t_l^I t_z^{II}) \right) \left( \tau_{ij} \frac{\delta(t_i^{II} t_j^I)}{\delta b_n} + \phi \frac{\partial \tau_{ij}}{\partial x_k} \frac{\delta x_k}{\delta b_n} t_i^{II} t_j^I \right) dS \\ & - \int_{S_W} \frac{\partial J_{S_W,k}}{\partial \tau_{lz}} n_k t_l^{II} t_z^{II} \left( \tau_{ij} \frac{\delta(t_i^{II} t_j^{II})}{\delta b_n} + \phi \frac{\partial \tau_{ij}}{\partial x_k} \frac{\delta x_k}{\delta b_n} t_i^{II} t_j^{II} \right) dS \end{aligned} \quad (4)$$

and  $\tau_{ij}^a$  are the components of the adjoint stress tensor.

Since, in the *FI* adjoint formulation,  $\phi = 0$ , the expression for  $W(\phi)$  is, in fact, quite simpler than that given by eq. 4 which was kept as general as possible so as to fit to all the adjoint

formulations discussed in section 1. In eq. 3,  $t_i^I, t_i^H$  are the components of the tangential to the surface unit vectors (in 3D shapes).

The *SI* which is often referred to as the "reduced-gradient" adjoint formulation [3], was developed later on and proved to be an attractive improvement. The *SI* adjoint formulation is based on the application of the Leibniz theorem for integral variations, namely

$$\frac{\delta L}{\delta b_n} = \frac{\delta J}{\delta b_n} + \int_{\Omega} \left( u_i \frac{\partial R_i^v}{\partial b_n} + q \frac{\partial R^p}{\partial b_n} \right) d\Omega + \int_S (u_i R_i^v + q R^p) n_k \frac{\delta x_k}{\delta b_n} dS \quad (5)$$

The last integral in eq. 5 is usually ignored, [9], by making the (debatable) assumption that the flow PDEs are satisfied along the boundary.

The *SI* formulation (i.e. the severed form of eq. 5) in shape optimization problems in fluid mechanics, governed by the same state equations as before, leads to the following SD expression

$$\frac{\delta J}{\delta b_n} \Big|_{SI} = \int_{S_w} \left[ - \left( \tau_{ij}^a n_j - q n_i + \frac{\partial J_{S_w, l}}{\partial v_i} n_l \right) \frac{\partial v_i}{\partial x_k} + \frac{\partial J_{S_w, i}}{\partial x_k} n_i \right] \frac{\delta x_k}{\delta b_n} dS + W(1) \quad (6)$$

Before proceeding to the new-third formulation and for better understanding its merits, the two formulations are compared. In eq. 3, one should notice the presence of the field integral containing the spatial gradient of the grid sensitivities which is the main difference between the *FI* and *SI* adjoint formulations. Their computation by finite differences (FD) is expensive for a large number of design variables. As a result, the *SI* formulation is, by far, less expensive than the *FI* formulation in problems with many design variables and, thus, preferred. However, because of the elimination of last integral in eq. 5, the accuracy of the *SI* formulation is not guaranteed. In contrast, the *FI* formulation provides accurate SD. To the authors knowledge, there is no other paper on continuous adjoint for turbulent flows dealing with the accuracy-problem of the *SI* formulation. Only a couple of them, [1, 8], refer to this problem in laminar and inviscid flows, without providing a solution at least based on a purely continuous approach.

The E-*SI* (Enhanced-*SI* adjoint) formulation, as firstly proposed in [5], intends to alleviate the accuracy issue of the *SI* formulation, while having almost the same computational cost. In other words, the E-*SI* combines the main advantages of the *FI* and *SI* formulations. In the E-*SI* formulation, in order to avoid the computation of  $\delta x_k / \delta b_n$  at the internal nodes, the adjoint formulation is extended by considering grid displacement PDEs as extra governing equations, i.e. extra constraints. Without loss in generality, we make the assumption that grid displacement (in fact, the adaptation to the varying boundaries of the domain) is performed by solving Laplace equations. These read  $R_i^m = \frac{\partial^2 m_i}{\partial x_j^2} = 0$  and, as extra constraints in the form of  $\int_{\Omega} m_i^a R_i^m d\Omega$ , should be added to the RHS of eq. 1. Here,  $m_i$  ( $i = 1, 2, 3$ ) are the Cartesian displacements of grid nodes and  $m_i^a$  is the adjoint to  $m_i$ . In order to eliminate the field integrals in  $\delta L / \delta b_n$ , which include  $\delta x_k / \delta b_n$ , the adjoint grid displacement PDEs

$$R_k^{m^a} = \frac{\partial^2 m_k^a}{\partial x_j^2} + \frac{\partial}{\partial x_j} \left\{ u_i v_j \frac{\partial v_i}{\partial x_k} + u_j \frac{\partial p}{\partial x_k} + \tau_{ij}^a \frac{\partial v_i}{\partial x_k} - u_i \frac{\partial \tau_{ij}}{\partial x_k} - q \frac{\partial v_j}{\partial x_k} \right\} = 0 \quad (7)$$

should be satisfied in addition to the adjoint meanflow (and turbulence model) PDEs (see section 2). Therefore, in E-*SI*, the gradient of J becomes

$$\frac{\delta J}{\delta b_n} \Big|_{E-SI} = \int_{S_w} \left[ - \left( \tau_{ij}^a n_j - q n_i + \frac{\partial J_{S_w, l}}{\partial v_i} n_l \right) \frac{\partial v_i}{\partial x_k} - \frac{\partial m_i^a}{\partial x_j} n_j + \frac{\partial J_{S_w, i}}{\partial x_k} n_i \right] \frac{\delta x_k}{\delta b_n} dS + W(1) \quad (8)$$

including solely boundary integrals. The extra cost of computing the gradient of J using eq. 8, instead of eq. 6, which accounts for the numerical solution of the adjoint grid displacement

equations, is negligible compared to that of solving the primal and adjoint PDEs. The two major advantages of the *SI* formulation are valid in *E-SI* too: (a) cost-independence from the number of design variables and (b) gradient computations based on surface integrals only. Note that, for the chosen grid displacement model, the solution of the (primal) grid displacement PDEs is not needed, yet only its adjoint equation must be solved after the solution of the adjoint to the flow model PDEs.

In figs. 1 and 2, the sensitivity derivatives computed by the three different adjoint formulations are compared in a laminar and a turbulent flow problem. The first case deals with the computation of the lift and drag SD of an isolated airfoil. The second case deals with the computation of the lift SD for the flow around an isolated airfoil at turbulent flow conditions. In both cases, the accuracy of the *E-SI* formulation in comparison with the less expensive and less accurate *SI* and the accurate though expensive *FI* is noticeable.

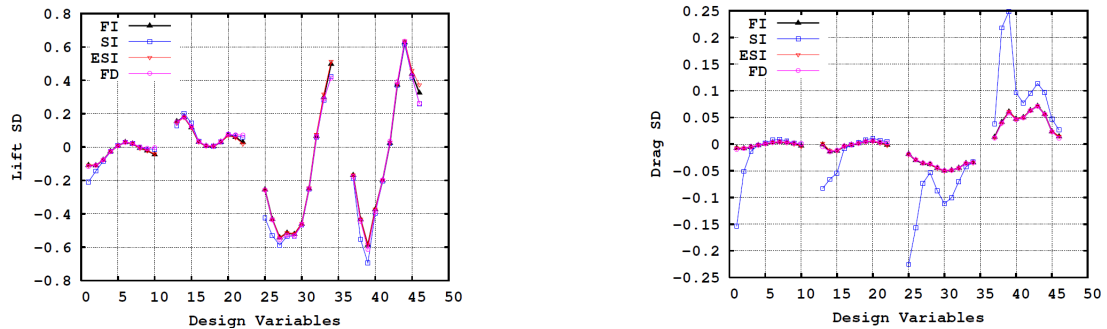


Figure 1: Laminar flow around an isolated airfoil designed for low drag at its 'nominal' operating point; however, here, this is studied at laminar flow conditions ( $Re=600$ ,  $\alpha_{\text{inf}}=3^\circ$ ): Comparison of the SD computed by the *FI*, *SI*, *E-SI* and *FD* methods for lift (left) and drag (right). SD are computed w.r.t. the  $x$  (first half points in the abscissa) and  $y$  (second half) coordinates of 24 NURBS control points parameterizing the pressure and suction sides. A *C*-type structured grid with 45000 cells is used. For the lift, all the adjoint formulations practically match the outcome of the *FD*. This is not, however, the case for the drag since the *SI* approach computes SD which deviate substantially from the *FD* whereas the *FI* and *E-SI* are in perfect agreement.

## 2 Continuous Adjoint to the Turbulence Model PDEs

In the literature of continuous adjoint, to compute the gradient of objective functions in turbulent flows governed by the RANS, it is common to neglect variations in the turbulent viscosity, by assuming that changes in the shape of the aerodynamic body affect only the mean flow quantities. This is referred to as the "frozen turbulence" assumption and leads to a system of adjoint equations which doesn't include the adjoint to the turbulence model PDEs. The so-computed SD are occasionally wrongly signed and this may seriously affect the descent process. A much more rigorous approach includes the differentiation of the turbulence model equation(s) w.r.t. the design variables and requires the formulation and solution of the adjoint to the turbulence model PDEs. At NTUA, the (continuous) adjoint PDEs for three turbulence models, namely the Spalart–Allmaras [13],  $k-\epsilon$  [12] and  $k-\omega$  SST [4] models have been developed.

Assuming, for instance, that closure is affected by the one-equation Spalart–Allmaras model the development of the adjoint *SI* formulation starts by adding  $\int_{\Omega} \tilde{\nu}_a R^{\tilde{\nu}} d\Omega$  to the RHS of eq. 1 where  $\tilde{\nu}_a$  is the adjoint to the model variable  $\tilde{\nu}$  and  $R^{\tilde{\nu}}$  is the residual of the Spalart–Allmaras equation. In the Launder–Sharma  $k-\epsilon$  or the  $k-\omega$  SST models, this new integral must be replaced

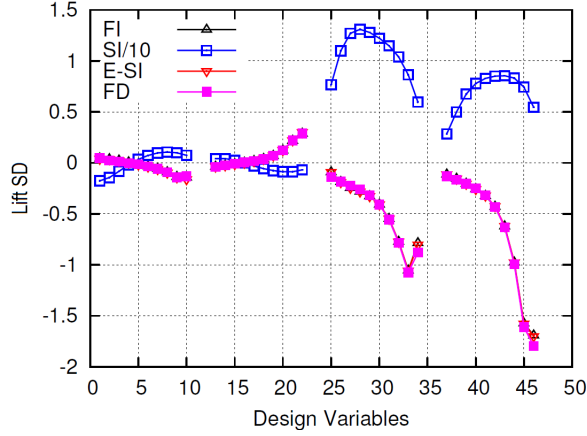


Figure 2: Turbulent flow around the NACA0012 airfoil ( $Re = 10^6$ ,  $a_{\text{inf}} = 3^\circ$ , average  $y^+ = 0.2$ ): Comparison of the lift SD computed by the FI, SI, E-SI and FD methods. Similar shape parameterization as in 1. The SI results have been divided by 10 in order to be on the same scale with those of the other methods. All adjoint variants presented include the complete differentiation of the turbulence model, see section 2. Despite the fact that the grid is adequately stretched for RANS computations based on low-Reynolds number turbulence models, the SI-based SD differ considerably from the FI ones or the FD and have the wrong sign for almost all design variables. In contrast, the E-SI approach computes the reference SD values, without the extra cost of the FI approach.

by  $\int_{\Omega} k_a R^k d\Omega + \int_{\Omega} \epsilon_a R^\epsilon d\Omega$  or  $\int_{\Omega} k_a R^k d\Omega + \int_{\Omega} \omega_a R^\omega d\Omega$  respectively, where the computation of the new adjoint fields requires the formulation and solution of extra PDEs. After zeroing the multipliers of  $\delta p / \delta b_n$ ,  $\delta v_i / \delta b_n$  and  $\delta \tilde{\nu} / \delta b_n$  (for the Spalart-Allmaras model), the adjoint PDEs arise. In the absence of field integrals in J, the system of the adjoint PDEs, for the Spalart-Allmaras model, becomes

$$R^q = -\frac{\partial u_j}{\partial x_j} = 0 \quad (9)$$

$$R_i^u = u_j \frac{\partial v_j}{\partial x_i} - \frac{\partial (v_j u_i)}{\partial x_j} - \frac{\partial}{\partial x_j} \left[ (\nu + \nu_t) \left( \frac{\partial u_i}{\partial x_j} + \frac{\partial u_j}{\partial x_i} \right) \right] + \frac{\partial q}{\partial x_i} + AMS_i = 0, \quad i = 1, 2, (3) \quad (10)$$

$$R^{\tilde{\nu}_a} = -\frac{\partial (v_j \tilde{\nu}_a)}{\partial x_j} - \frac{\partial}{\partial x_j} \left[ \left( \frac{\nu + \tilde{\nu}}{\sigma} \right) \frac{\partial \tilde{\nu}_a}{\partial x_j} \right] + \frac{1}{\sigma} \frac{\partial \tilde{\nu}_a}{\partial x_j} \frac{\partial \tilde{\nu}}{\partial x_j} + 2 \frac{c_{b2}}{\sigma} \frac{\partial}{\partial x_j} \left( \tilde{\nu}_a \frac{\partial \tilde{\nu}}{\partial x_j} \right) + \tilde{\nu}_a \tilde{\nu} C_{\tilde{\nu}} + \frac{\partial \nu_t}{\partial \tilde{\nu}} \frac{\partial u_i}{\partial x_j} \left( \frac{\partial v_i}{\partial x_j} + \frac{\partial v_j}{\partial x_i} \right) + (-P(\tilde{\nu}) + D(\tilde{\nu})) \tilde{\nu}_a = 0 \quad (11)$$

where  $P(\tilde{\nu})$  and  $D(\tilde{\nu})$  are the production and dissipation terms of the model; among other,  $D(\tilde{\nu})$  depends on the distance  $\Delta$  from the wall. The extra terms  $AMS_i$  in eq. 10 arise from the differentiation of the turbulence model [13, 10] and would not exist if the "frozen turbulence" assumption was made; these terms quantify the effect of the adjoint turbulence on the adjoint mean-flow equations. The adjoint boundary conditions are derived by properly treating the boundary integrals that depend on the variations in the flow variables. After satisfying the field adjoint equations and boundary conditions,  $\delta J / \delta b_n$  becomes

$$\frac{\delta J}{\delta b_n} \Big|_{SI} = \int_{S_W} \left[ -\left( \tau_{ij}^a n_j - q n_i + \frac{\partial J_{S_W, l}}{\partial v_i} n_l \right) \frac{\partial v_i}{\partial x_k} + \frac{\partial J_{S_W, i}}{\partial x_k} n_i \right] \frac{\delta x_k}{\delta b_n} dS + W(1) + TMT \quad (12)$$

where  $TMT$  stands for extra terms that depend on the turbulence model which, in the Spalart-Allmaras model, becomes  $TMT = \int_{S_W} \left\{ \left[ -\left( \nu + \frac{\tilde{\nu}}{\sigma} \right) \frac{\partial \tilde{\nu}_a}{\partial x_j} n_j + \frac{\partial J_{S_k}}{\partial \tilde{\nu}} n_k \right] \frac{\partial \tilde{\nu}}{\partial x_k} + \tilde{\nu}_a R^{\tilde{\nu}} \right\} \frac{\delta x_k}{\delta b_n} dS$ . Note

that, without loss in generality, the *SI* adjoint formulation has been adopted. To account for the differentiation of the distance  $\Delta$  from the wall, i.e. to take into consideration  $\delta\Delta/\delta b_n$ , the Hamilton-Jacobi equation ( $R_\Delta = \frac{\partial(c_j\Delta)}{\partial x_j} - \Delta \frac{\partial^2\Delta}{\partial x_j^2} - 1 = 0$ , where  $c_j = \partial\Delta/\partial x_j$ ) is used as the PDE governing  $\Delta$  [2]. Then, the objective function is extended by adding  $\int_\Omega \Delta_a R^\Delta d\Omega$  in eq. 1 and a new adjoint PDE, in the form of  $R^{\Delta_a} = -2\frac{\partial}{\partial x_j} \left( \Delta_a \frac{\partial\Delta}{\partial x_j} \right) + \tilde{\nu}\tilde{\nu}_a C_\Delta = 0$ , for the adjoint distance  $\Delta_a$ , is derived and solved. In such a case, the TMT is further expanded by the term  $\int_{S_W} \left( -2\Delta_a \frac{\partial\Delta}{\partial x_j} n_j \frac{\partial\Delta}{\partial x_k} + \Delta_a R^\Delta \right) \frac{\delta x_k}{\delta b_n} dS$ . A convincing example demonstrating the need of solving the adjoint turbulence model equations can be found in fig. 3.

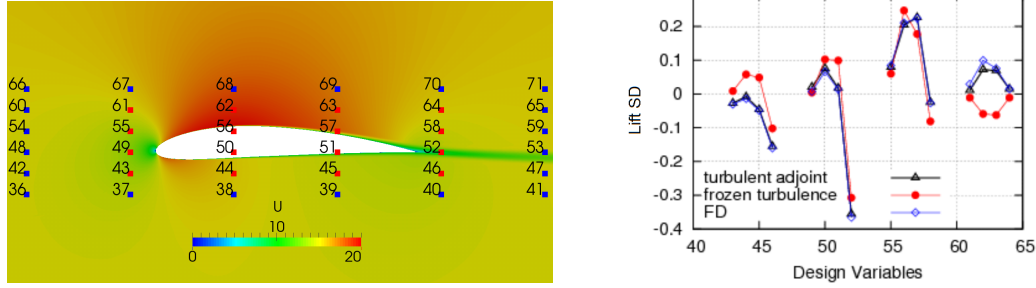


Figure 3: Turbulent flow around a NACA4412 isolated airfoil ( $Re = 1.5 \times 10^6$ ,  $a_{\text{inf}} = 0^\circ$ ). A grid with 60000 cells is used, with an average  $y^+$  value of the first cell centers off the wall of 0.03. Adjoint to the low-Re Spalart-Allmaras model: Left: velocity magnitude field. A volumetric B-Splines morpher is used to parameterize the airfoil. The structured control grid of the morpher is plotted on top of the airfoil, along with the ID of each control point. The blue control points are kept fixed and only the red ones are allowed to vary. Right: drag SD w.r.t. the  $y$  displacements of the control points. Three SD distributions are compared by solving the complete adjoint approach (marked as “turbulent adjoint”), by making the “frozen turbulence” assumption and by FD. The abscissa stands for the control point IDs. By making the “frozen turbulence” assumption, wrongly signed SD are computed for the control points 43 to 45 and 61 to 64.

Since, in the industry there is a need to use less stretched grids than those required by the low-Re turbulence models, the development of the continuous adjoint method to turbulence models which use wall functions on coarser meshes and the law of the wall appears to be of value. The adjoint to three models supported by wall functions, namely the  $k-\epsilon$  [15], Spalart-Allmaras [10] and  $k-\omega$  SST ones has been developed and tested. This has led to the adjoint equations and boundary conditions expressed in terms of the adjoint to the friction velocity which is used to bridge the gap between the solid wall and the first grid node off the wall.

### 3 Automotive Applications

In this section, two automotive applications are presented. In the first one, the drag minimization of one DrivAer car model configuration, developed by the Institute of Aerodynamics and Fluid Mechanics of TU Munich, is demonstrated in figs 4, 5 and 6 with description and comments in the captions. The Spalart-Allmaras model with wall functions was used to effect closure; the computational grid consists of about 3.8 million cells. The second case is concerned with the VW Polo passenger car. Using the DES variant of the Spalart-Allmaras turbulence model with wall functions, the minimization of two objective functions (total and rear lift) is separately studied and the computed sensitivity maps (considered as the roadmap to the optimal solutions) are presented, leading to a very interesting comparison of trends, see fig. 7.

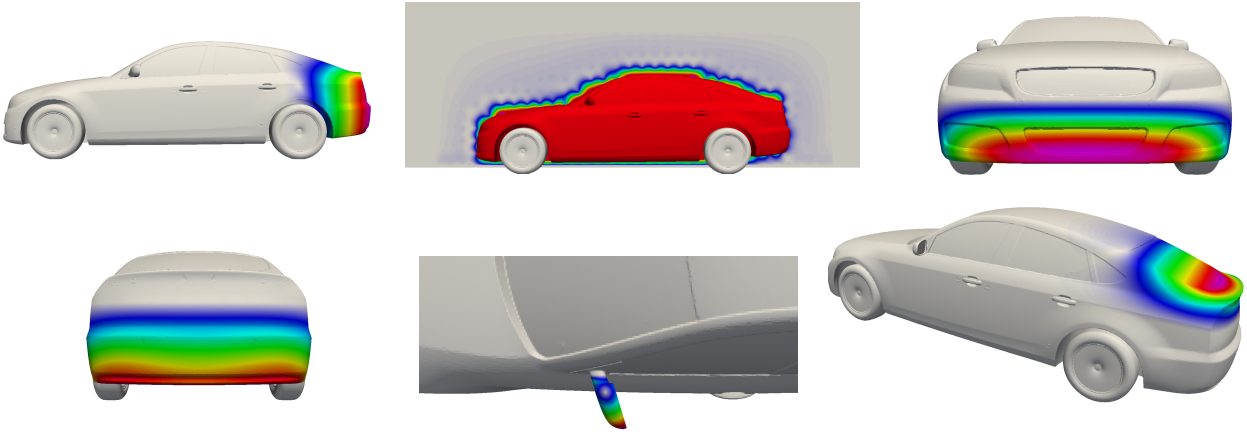


Figure 4: DrivAer car (fast-back configuration with smooth underbody, with mirrors and wheels) shape optimization for drag minimization: Six design parameters are used to morph six different parts of the car, by distinctly controlling: the boat tail (top-left), the car height (top-middle), the front bumper (top-right), the rear bumper (bottom-left), the shape of the mirror (bottom-middle), the shape of the rear window (bottom-right). In color, one may see  $\delta x_k / \delta b_n$ .

#### 4 Adjoint Methods for Topology Optimization

Continuous adjoint methods for solving topology optimization problems for laminar and turbulent ducted flows of incompressible fluids, with or without heat transfer, have been developed, [7, 11]. For turbulent flows, the adjoint approach includes the differentiation of the turbulence model, as already discussed in section 2. In cases where geometries with more than one outlet channels are studied, constraints on (a) the percentage of the incoming flow rate, (b) the swirl and (c) the temperature distribution at each exit boundary can optionally be imposed.

In fig. 8, the optimization of an air-conditioning duct, transferring air from the main console to the back seats of a passenger car is investigated, targeting minimum total pressure losses. The case is part of the E.C. project “Flowhead” and was provided by Volkswagen AG. The flow is modeled using the Spalart–Allmaras model with wall functions. The optimization led to a 45% decrease in total pressure losses.

In order to maintain an explicit description of the solid-fluid interface, the topology optimization process is enhanced using the level set method. This also helps preventing the formation of undesirable fluid or solid islands.

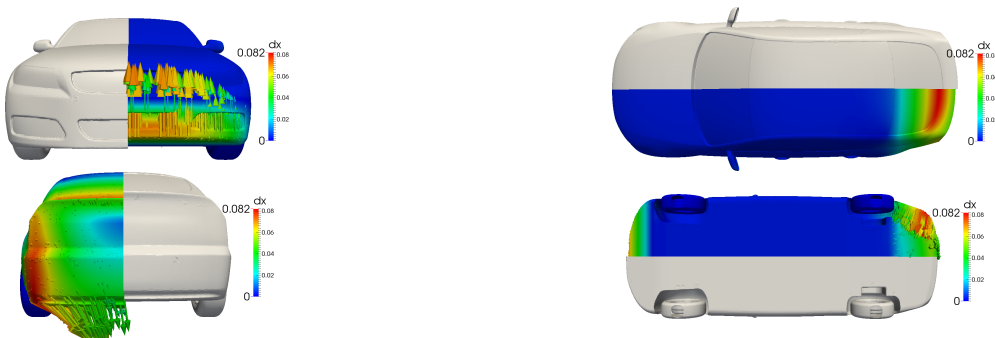


Figure 5: DrivAer car shape optimization for drag minimization: initial (starboard side) and optimized (port side) car geometries, coloured based on the cumulative deformation of the car surface after 15 optimization cycles. The areas with the highest deformation are those affected by the boat-tail and rear-windshield shape design parameters.

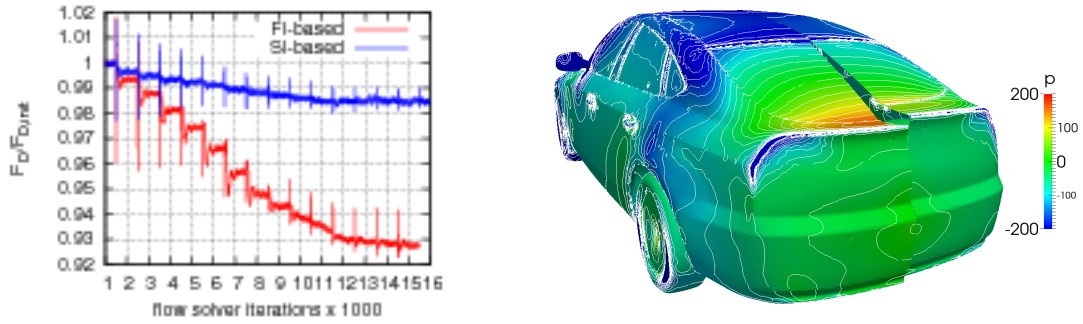


Figure 6: *DrivAer* car shape optimization for drag minimization: Left: Evolution of the normalized drag in terms of the number of iterations of the flow solver, following the FI and SI adjoint formulations. In each optimization cycle, the flow solver runs for 1000 iterations (since a previously “converged” solution was used to initialize the optimization; in the first optimization cycle, the stopping criterion was set to 500 iterations). Kinks in the objective function value indicate the first iterations after each shape update. With the FI formulation, a drag reduction by 7% was achieved whereas the SI gave no more than 1.5% reduction. Right: initial (starboard) and optimized (port) (with the FI formulation) geometries, coloured based on the computed surface pressure. Lowering the rear windshield, creating a spoiler at the end of the trunk and a boat-tail shaped rear side led to increased pressure on the rear part of the car and, thus, lower drag.

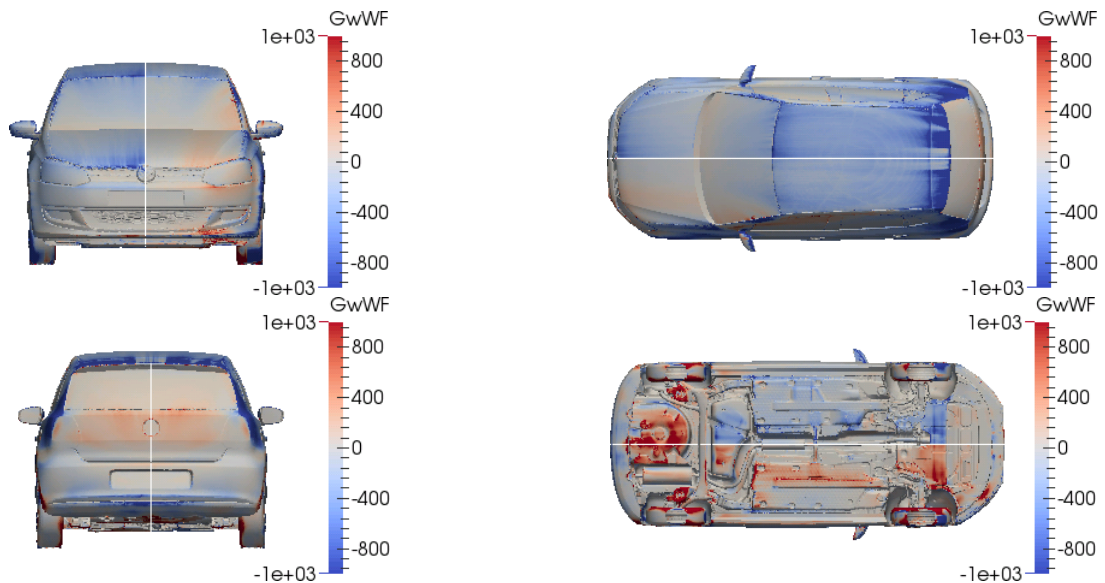


Figure 7: *VW Polo* passenger car. Sensitivity maps for the rear and total lift minimization. Combined views of the sensitivity maps for the rear (starboard) and the total lift (port). Red/blue areas suggest inward/outward displacement, respectively. With different targets, opposite trends (particularly in the front part of the car) are observed.

Current research aims at a novel transitional process that, starting from the adjoint topology solutions, generates a NURBS parameterized surface which can be used either as a CAD-compatible solution to topology or as the initial shape for the shape optimization loop, in the framework of a combined topology-shape optimization algorithm [6].

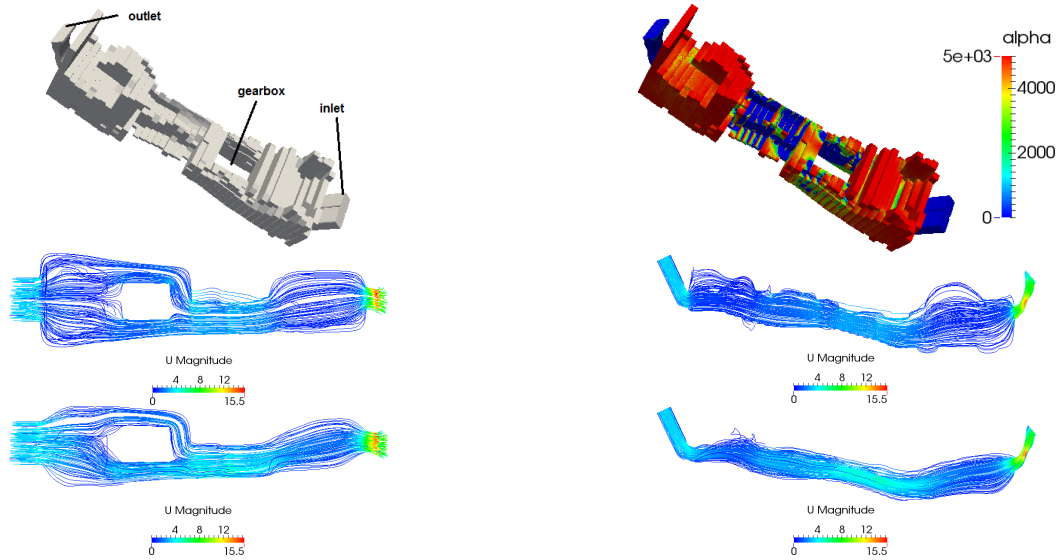


Figure 8: Topology optimization of a car air-conditioning duct targeting minimum total pressure losses. The domain includes the inlet and outlet ducts that remain unchanged through the optimization process and the design space for the main body of the duct. The hole in the middle of the domain is the space reserved for the gear lever. The grid consists of about 5.5 million cells, the Reynolds number based on the inlet hydraulic diameter is  $Re \approx 3000$ . Top-left: duct geometry. Top-right: computed porosity field at the last optimization cycle. Red areas correspond to the solidified part of  $\Omega$ . Middle: Streamlines computed in the domain without any porosity-based blockage/solidification. Intense flow recirculation occurs close to the inlet duct, where the cross-section area increases abruptly. In addition, there is no clear path to lead the flow to the outlet duct. As a result, the flow recirculates close to the outlet area, leading to high losses. Bottom: Flow velocity streamlines computed in the optimized geometry. The optimisation made the cross-section of the duct near the inlet smaller, in order to minimize recirculation. In addition, a clear path connecting the body of the design space with the outlet ducts has been formed, in order to smoothly steer the flow towards the back seats of the car.

## References

- [1] W.K. Anderson and V. Venkatakrishnan. Aerodynamic design optimization on unstructured grids with a continuous adjoint formulation. *Computers & Fluids*, 28(4-5):443–480, 1999.
- [2] A. Bueno-Orovio, C. Castro, F. Palacios, and E. ZuaZua. Continuous adjoint approach for the Spalart–Allmaras model in aerodynamic optimization. *AIAA Journal*, 50(3):631–646, 2012.
- [3] A. Jameson and S. Kim. Reduction of the adjoint gradient formula in the continuous limit. In *AIAA Paper 2003-0040, 41th Aerospace Sciences Meeting and Exhibit*, Reno, Nevada, January 2003.
- [4] I.S. Kavvadias, E.M. Papoutsis-Kiachagias, G. Dimitrakopoulos, and K.C. Giannakoglou. The continuous adjoint approach to the  $k-\omega$  SST turbulence model with applications in shape optimization. *Engineering Optimization*, 47(11):1523–1542, 2015.
- [5] I.S. Kavvadias, E.M. Papoutsis-Kiachagias, and K.C. Giannakoglou. On the proper treatment of grid sensitivities in continuous adjoint methods for shape optimization. *Journal of Computational Physics*, 301:1–18, 2015.

- [6] J.R.L. Koch, E.M. Papoutsis-Kiachagias, and K.C. Giannakoglou. Transition from 2D continuous adjoint level set topology to shape optimization. In *ECCOMAS 2016, VII European Congress on Computational Methods in Applied Sciences and Engineering*, Crete Island, Greece, June 5-10 2016.
- [7] E.A. Kontoleontos, E.M. Papoutsis-Kiachagias, A.S. Zymaris, D.I. Papadimitriou, and K.C. Giannakoglou. Adjoint-based constrained topology optimization for viscous flows, including heat transfer. *Engineering Optimization*, 45(8):941–961, 2013.
- [8] C. Lozano. Discrete surprises in the computation of sensitivities from boundary integrals in the continuous adjoint approach to inviscid aerodynamic shape optimization. *Computers & Fluids*, 56:118–127, 2012.
- [9] D.I. Papadimitriou and K.C. Giannakoglou. A continuous adjoint method with objective function derivatives based on boundary integrals for inviscid and viscous flows. *Journal of Computers & Fluids*, 36(2):325–341, 2007.
- [10] E.M. Papoutsis-Kiachagias and K.C. Giannakoglou. Continuous adjoint methods for turbulent flows, applied to shape and topology optimization: Industrial applications. *Archives of Computational Methods in Engineering*, 23:255–299, June 2016.
- [11] E.M. Papoutsis-Kiachagias, E.A. Kontoleontos, A.S. Zymaris, and K.C. Giannakoglou. Constrained topology optimization for laminar and turbulent flows, including heat transfer. In *EUROGEN 2011, International Conference on Evolutionary and Deterministic Methods for Design, Optimization and Control with Applications to Industrial and Societal Problems*, Capua, Italy, September 14-16 2011.
- [12] E.M. Papoutsis-Kiachagias, A.S. Zymaris, I.S. Kavvadias, D.I. Papadimitriou, and K.C. Giannakoglou. The continuous adjoint approach to the  $k-\epsilon$  turbulence model for shape optimization and optimal active control of turbulent flows. *Engineering Optimization*, 47(3):370–389, 2015.
- [13] A.S. Zymaris, D.I. Papadimitriou, K.C. Giannakoglou, and C. Othmer. Continuous adjoint approach to the Spalart-Allmaras turbulence model for incompressible flows. *Computers & Fluids*, 38(8):1528–1538, 2009.
- [14] A.S. Zymaris, D.I. Papadimitriou, K.C. Giannakoglou, and C. Othmer. Adjoint wall functions: A new concept for use in aerodynamic shape optimization. *Journal of Computational Physics*, 229(13):5228–5245, 2010.
- [15] A.S. Zymaris, D.I. Papadimitriou, K.C. Giannakoglou, and C. Othmer. Adjoint wall functions: A new concept for use in aerodynamic shape optimization. *Journal of Computational Physics*, 229(13):5228–5245, 2010.